Acta Cryst. (1965). **18**, 45

Calculation of Transmission Factors in Crystals with any Polygonal Cross-section and High Absorption Power

By Adolfo Ferrari, Antonio Braibanti and Antonio Tiripicchio

Istituto di Chimica generale della Università di Parma, Italy

(*Received* 27 *June* 1962 *and in revised form* 30 *December* 1963)

The cross-section of an absorbing crystal is divided into a mosaic, each area of which is uniquely defined by the faces through which pass the rays that are incident on and diffracted from that area. For strongly absorbing media only a few of these areas on the surface contribute significantly to the transmission factor; the remaining regions are assumed to give approximately null contribution. The contribution of each area is defined as an *equivalent diffracting area* (*e.d.a.*). The *e.d.a.* of each surface area is easy to compute and has a simple physical interpretation related to the locus of constant path-length for which $\mu l = 1$. A vectorial representation of the cross-sectional profile facilitates selection of the appropriate *e.d.a.* formulae, and makes the whole calculation equally convenient for evaluation graphically or by a computer. Extension of the procedure to crystals in three dimensions is also considered.

Introduction

Methods of evaluating absorption corrections fall into three main groups:

(1) Tabular or simple analytical procedures applicable to spherical, ellipsoidal or cylindrical crystals or to certain simply shaped polyhedra, slabs, *etc.* (Bradley, 1935; Evans, 1952; Evans & Ekstein, 1952; Frasson, 1958; Frasson & Bezzi, 1958, 1959; Bond, 1959; Fitzwater, 1961).

(2) Sampling methods, applicable only to crystals of low or medium absorption. Any cross-section can be tackled graphically (Albrecht, 1939; Joel, Vera & Garaycochea, 1953; Rogers & Moffett, 1956; Henshaw, 1958; Frasson, 1958; Frasson & Bezzi, 1958, 1959), but a computer can only conveniently cope with polyhedra (Busing & Levy, 1957; Wells, 1960).

(3) Block mosaic methods, which are applicable to any polygonal cross-section but are particularly convenient for strongly absorbing specimens. The methods described by Hendershot (1937), Howells (1950), Carazzolo & Mammi (1956) and Grdenić (1949, 1952, 1956) look at first sight as though the graphical procedure needed for each reflexion is so individualistic as to make it impracticable to transfer it to a computer. It has been shown, however (Ferrari, Braibanti & Tiripicchio, 1961, 1963) how the procedure for square or rectangular profiles could be systematized. This paper extends that study to present a general treatment for prisms of uniform convex polygonal cross-section and outlines its extension to crystals of any shape with no reentrant angles.

Preliminary considerations

The transmission factor is usually defined as the dimensionless quantity

$$A_\tau = \frac{1}{\tau}\int_\tau \exp(-\mu l)\,d\tau ,$$

where τ represents either a volume or area. It can be thought of as the ratio between the *equivalent diffracting volume* (*e.d.v.*) or area (*e.d.a.*),

$$\tau_e = \int_\tau \exp(-\mu l)\,d\tau$$

and the total volume or area τ. When absorption is high and much of the interior of the crystal is screened from the radiation the *e.d.a.* will be shown to have a simple physical interpretation and correspondingly simple formulae.

In view of the fact that each reflexion is recorded twice (*e.g.* in the Weissenberg camera once in the upper and again in the lower part of the photograph (Fig. 1(*a*), (*b*)), we must be able to specify the orientation of the crystal with respect to the camera. This can be done by reference to an orthogonal set of right-handed axes defined by a 'reference plane' of the crystal and some axis in the X-ray equipment. To be explicit, the 'reference plane' can be either an external face or a readily identifiable lattice plane. The z axis is taken parallel to the rotation axis of the crystal, positively away from the goniometer head. The 'reference face' or plane must be parallel to z, and x positive is taken along its outward face-normal; y is then defined by the right-handed system (see Fig. 1). In this system of axes the angles are measured positive if *anticlockwise* when looking along $+z$ toward 0; in a more general statement they are considered positive in the sense $x \to y$, $y \to z$ and $x \to z$.

As shown in Fig. 1(*a*), (*b*), (*c*), (*d*), we must preserve a clear distinction between a left-handed or anticlockwise deflection (2θ positive) corresponding to

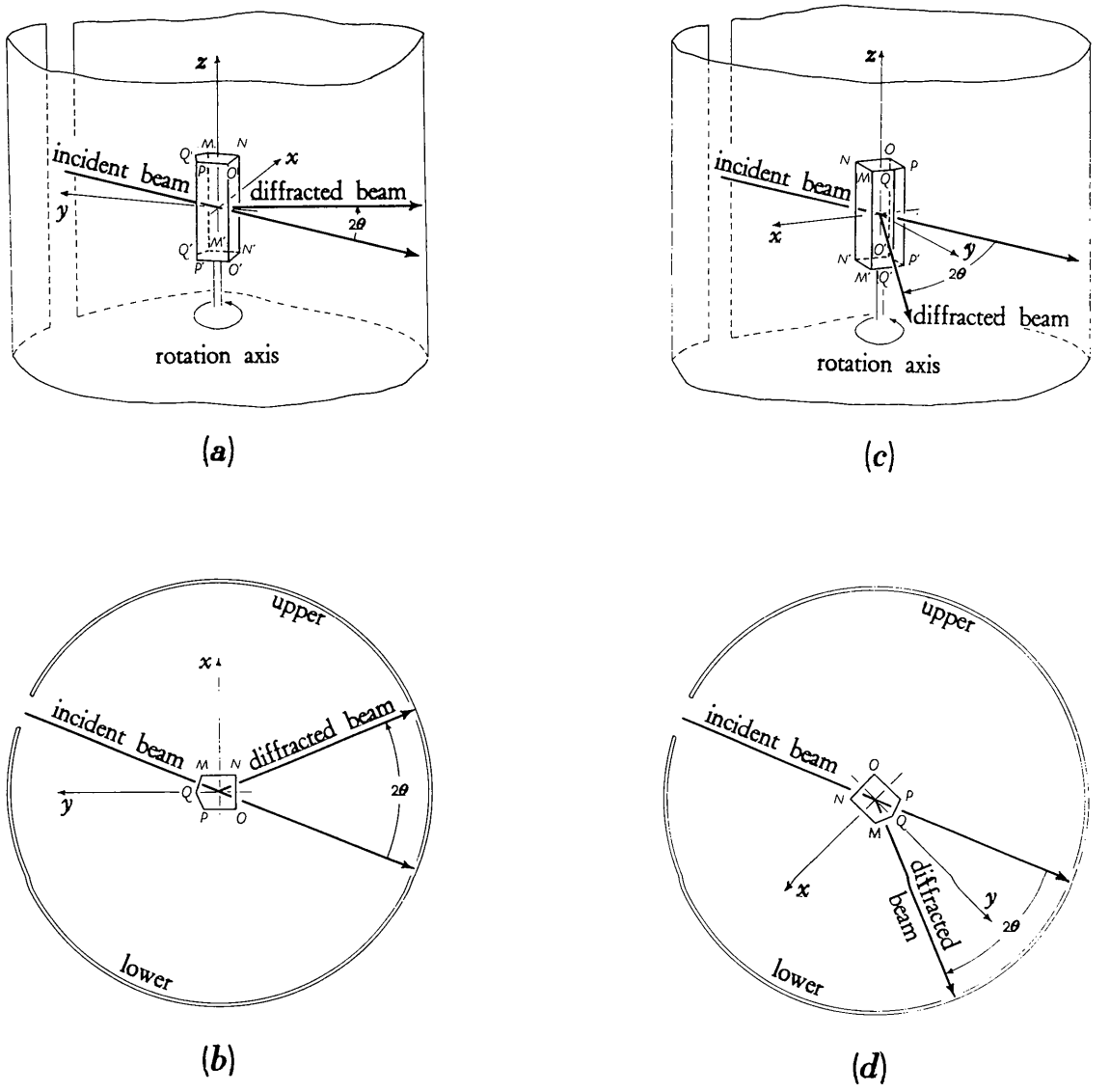

Fig. 1. Position of the crystal in a Weissenberg camera: (*a*), (*b*) Left-hand deflection. (*c*), (*d*) Right-hand deflection.

spots recorded on the upper part of the photograph and a right-handed or clockwise deflection (2θ negative) corresponding to spots recorded on the lower part of the photograph.

Vectorial representation

The unit vectors **i** and **d** (Fig. 2) denote the actual directions of the incident and diffracted rays and the unit vectors $-\mathbf{i}$ and $-\mathbf{d}$ the opposite directions. Then, for a left-handed deflection (Fig. 2(*a*)), the unit vector $\mathbf{t}_{hk0}=-(\mathbf{i}+\mathbf{d})/2\cos\theta$ represents the reticular plane $hk0$, the unit vector $\mathbf{n}_{hk0}=(\mathbf{d}-\mathbf{i})/2\sin\theta$ represents the normal to the reticular plane $hk0$; for the reference plane, these vectors are called $\mathbf{t}_0$ and $\mathbf{n}_0$ and correspond to the $+y$ and $+x$ directions respectively. For a right-handed deflection (Fig. 2(*b*)), the plane $hk0$ is defined by the unit vector $\mathbf{t}_{hk0}=(\mathbf{i}+\mathbf{d})/2\cos\theta$ and its normal by the unit vector $\mathbf{n}_{hk0}=(\mathbf{d}-\mathbf{i})/2\sin\theta$; for the reference plane $\mathbf{t}_0$ and $\mathbf{n}_0$ are again the $+y$ and $+x$ directions respectively.

The contour of the cross-section of the crystal can also be defined by vectors. Consider the polygonal cross-section shown in Fig. 3(*a*). To agree with the convention of measuring angles positive if anticlockwise, we number the corners consecutively, P_j, in an anticlockwise sense, starting from corner P_1. The consecutive face vectors $\mathbf{f}_j=\overrightarrow{P_{j-1}P_j}$ (*N.B.* $\mathbf{f}_j$ terminates at P_j) appear in Fig. 3(*b*) as an anticlockwise succession of radiating vectors, called the 'face vector fan'. If the $\mathbf{t}_{hk0}$'s corresponding to the real faces are called $\mathbf{t}_j$, then $\mathbf{f}_j=\mathbf{t}_j f_j$, where f_j is the width of the

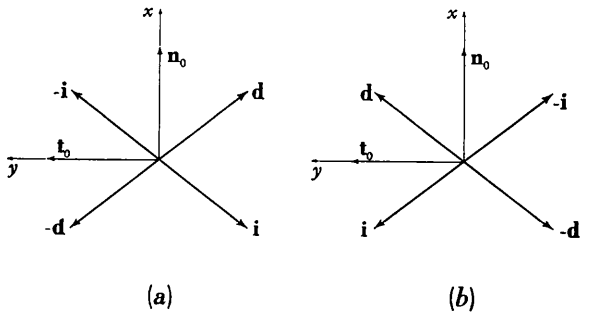

Fig. 2. Vectorial representation of reflexion from the reference plane:

(*a*) Left-hand deflection. (*b*) Right-hand deflection.

The unit vectors $\mathbf{t}_0$ and $\mathbf{n}_0$ represent the reference plane and its normal respectively. The unit vectors **i** and **d** represent the directions of the incident and diffracted rays, $-\mathbf{i}$ and $-\mathbf{d}$ the opposite directions.

corresponding face; the unit vectors $\mathbf{t}_j$ are more suitable for use in the vector fan. The faces can also be represented as in Fig. 3(*c*) by a similar anticlockwise succession of unit vectors $\mathbf{n}_j$, representing the face normals and called the 'face-normal vector fan'. It is convenient to make all angular measurements from the normal to the reference plane. The

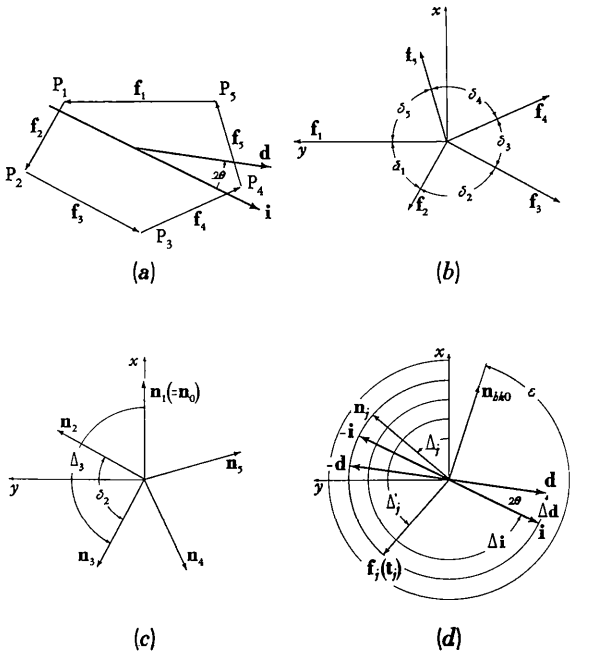

Fig. 3. Vectorial representation of the contour of the crystal cross-section (a left-hand deflection is assumed):

(*a*) Cross-section of the crystal. (*b*) Face vector fan. (*c*) Face normal vector fan. (*d*) Angles defining vectors $\mathbf{t}_j$, $\mathbf{n}_j$, **i**, **d**, and $\mathbf{n}_{hk0}$.

other face normals then occur at fixed and known angles Δ_j from $\mathbf{n}_0$ (Fig. 3(*d*)), while the set of $\mathbf{f}_j$ (or $\mathbf{t}_j$) vectors occur at $\Delta'_j = \Delta_j + \pi/2$. Although $\mathbf{n}_0$ and $\mathbf{n}_1$ *can* coincide, the distinction must be preserved if the reference plane is chosen as a lattice plane and has no corresponding external face. The external angle at P_j is δ_j.

The orientation of the diffracting planes is most readily calculated as ε, the angle (positive) in reciprocal space between the reciprocal lattice vector σ_{hk0} and $\mathbf{n}_0$. The angles Δ_j are particular values of ε, corresponding to the planes $(hk0)$ of the contour.

The angular orientations (reckoned from $\mathbf{n}_0$) of **i**, **d**, $-\mathbf{i}$, $-\mathbf{d}$ for any $hk0$ reflexion are:

	Left-hand deflection	Right-hand deflection
$\Delta_{\mathbf{i}}$	$\varepsilon-\pi/2-\theta$	$\varepsilon+\pi/2+\theta$
$\Delta_{\mathbf{d}}$	$\varepsilon-\pi/2+\theta$	$\varepsilon+\pi/2-\theta$
$\Delta(-\mathbf{i})$	$\varepsilon+\pi/2-\theta$	$\varepsilon-\pi/2+\theta$
$\Delta(-\mathbf{d})$	$\varepsilon+\pi/2+\theta$	$\varepsilon-\pi/2-\theta$

The grazing angles of incidence and emergence for face j are defined (Fig. 4(*a*)) as the angles between

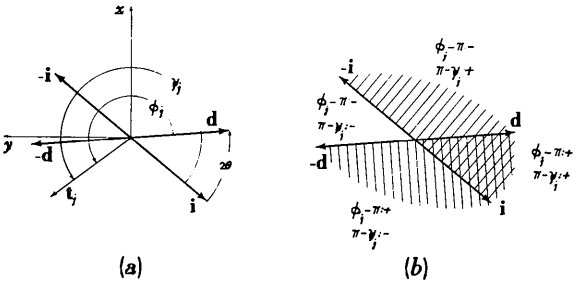

Fig. 4. Left-hand deflection:

(*a*) Grazing angles of incidence and emergence for face j. (*b*) Angular segments in which a vector fan is subdivided by **i**, **d**, $-\mathbf{i}$ and $-\mathbf{d}$; region not shaded is 'illuminated' by the X-rays.

$\mathbf{f}_j$ (or $\mathbf{t}_j$) and the vectors **i** and **d**, and written as ψ_j, φ_j respectively. Values for $(hk0)$ are:

	Left-hand deflection	Right-hand deflection
ψ_j	$\pi+\Delta_j-\varepsilon+\theta$	$\Delta_j-\varepsilon+\theta$
φ_j	$\pi+\Delta_j-\varepsilon-\theta$	$\Delta_j-\varepsilon-\theta$

Obviously only those faces are illuminated by the incident rays for which

$$\pi < \psi_j < 2\pi$$

and similarly only those can emit diffracted rays for which

$$0 < \varphi_j < \pi .$$

These conditions are indicated by shading in Fig. 4(*b*), to give four distinct angular segments:

(1) Face vectors $\mathbf{f}_j$, falling in the sector $-\mathbf{i}$, $-\mathbf{d}$, are 'exposed' to both **i** and **d** rays; $\mathbf{f}_j$ in this sector have both $\pi-\psi_j$ and $\varphi_j-\pi$ negative.

(2) Sector $-\mathbf{d}, \mathbf{i}$ is a region of 'penumbra' and $\mathbf{f}_j$ in this have $\pi-\psi_j$ negative and $\varphi_j-\pi$ positive.

(3) Sector $\mathbf{i}, \mathbf{d}$ is in shadow to both incident and diffracted rays; $\mathbf{f}_j$ in this sector have both $\pi-\psi_j$ and $\varphi_j-\pi$ positive.

(4) Sector $\mathbf{d}, -\mathbf{i}$ is a region of 'penumbra' and $\mathbf{f}_j$ in this sector have $\pi-\psi_j$ positive and $\varphi_j-\pi$ negative.

Throughout any practical problem the list of values of Δ_j is constant, and can be quickly converted to corresponding lists of ψ_j's and φ_j's as each new reflexion is treated. From these, short lists can be drawn up of the faces illuminated by **i** rays and emitting **d** rays. It is evident from the sequential numbering that the faces in each short list will be contiguous (in a cyclic sense).

Block mosaic and path length

If we now, according to Hendershot (1937), draw sets of **i** and **d** rays through the extremities of each of the faces, we produce (Fig. 5) a mosaic of parallelograms more than covering the whole crystal. Each mosaic block $(a_{p,q})$ is characterized by having all optical paths enter the crystal *via* face p and leave the crystal *via* face q. Each mosaic block contributes its own $e.d.a._{p,q}$ to the total. Thus $\tau_e = \sum_p \sum_q e.d.a._{p,q}$, and the evaluation of each $e.d.a._{p,q}$ entails a precise integration, which can be made exactly only when the path l of the X-rays inside each block is expressed in a linear form. In an orthogonal system of axes, the path length can be expressed by

$$l = a(x_P - x) + b(y_P - y)$$

where a and b are certain coefficients, x_P, y_P are the coordinates of a corner of a section and x, y are the

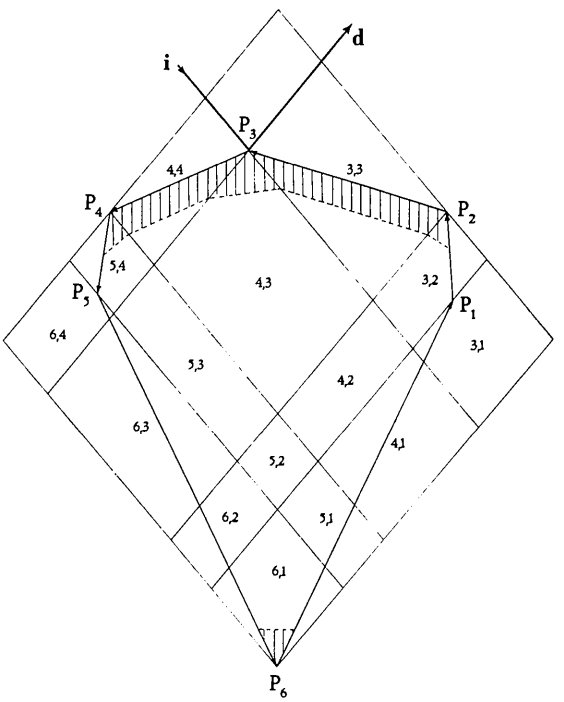

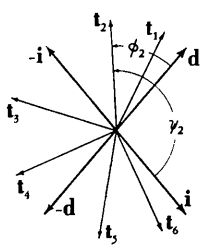

Fig. 5. Block mosaic of a cross-section. The shaded area indicates approximately the shape of the *e.d.a.*'s.

Table 1. *Equivalent diffracting areas (e.d.a.) for the six principally contributing types of mosaic block*

Formulae are quoted for left-handed $(+2\theta)$ deflection

Symbol	Type of block	Conditions in faces vector fan: Sector $-\mathbf{i}, -\mathbf{d}$	$-\mathbf{d}, \mathbf{i}$	$\mathbf{i}, \mathbf{d}$	$\mathbf{d}, -\mathbf{i}$	*e.d.a.* (cm²)
F_j	a_{jj}	t_j				$\frac{1}{\mu^2}\frac{\sin\psi_j \sin\varphi_j}{\sin\psi_j - \sin\varphi_j}\left\{L_j + \frac{\sin 2\theta}{\sin\psi_j - \sin\varphi_j}\right\}$
I_j	$a_{j+1,j}$	t_j t_{j+1}				$-\frac{1}{\mu^2}\frac{\sin\varphi_j \sin\psi_{j+1} \sin 2\theta}{(\sin\psi_j - \sin\varphi_j)(\sin\psi_{j+1} - \sin\varphi_{j+1})}$
S_j'	$a_{j+1,j}$	t_j	t_{j+1}			$\frac{1}{\mu^2}\frac{\sin^2\varphi_j}{\sin\psi_j - \sin\varphi_j}\frac{\sin\psi_{j+1}}{\sin\delta_j}$
S_j''	$a_{j+1,j}$	t_{j+1}			t_j	$\frac{1}{\mu^2}\frac{\sin^2\psi_{j+1}}{\sin\varphi_{j+1} - \sin\psi_{j+1}}\frac{\sin\varphi_j}{\sin\delta_j}$
C_j'	$a_{j+1,j}$		t_{j+1}		t_j	$-\frac{1}{\mu^2}\frac{\sin\varphi_j \sin\psi_{j+1}}{\sin\delta_j}$
C_j''	$a_{j,j+1}$		t_j		t_{j+1}	$-\frac{1}{\mu^2}\frac{\sin\psi_j \sin\varphi_{j+1}}{\sin\delta_j}$

coordinates of any point lying inside a block. The system of axes can be rotated or changed for convenience.

The most convenient system of axes, for strongly absorbing crystals, is that which makes the path dependent on one variable only. In fact this corresponds to applying the constant-path method (Howells, 1950) and provides a very simple physical interpretation of each $e.d.a._{p,q}$.

When μ is large only a few mosaic blocks, mainly on the irradiated side of the crystal, make any significant contribution. There are only a few distinct cases to consider. Simple tests suffice for selecting the formula appropriate to each mosaic block.

They are trigonometric functions of $\psi_j, \varphi_j, \theta$ and of the corner angles, δ_j, so the evaluation of τ_e is thereby reduced to the evaluation and summing of a few (rarely more than six) relatively simple formulae. The formulae are listed in Table 1 and derived in the Appendix.

Here we describe the notation and give a physical interpretation of the contributing *e.d.a.*'s. It should be noted that, because of the reversibility of ray paths, the *e.d.a.*'s for $(hk0)$ are the same for right- and left-handed deflections. Thus all formulae have to be symmetrical with respect to the interchange of ψ and φ, due attention being paid to changes of subscripts and angular constants. In Table 1 they are quoted for left-hand (2θ positive) deflections. Note that $\bar{h}\bar{k}0$ entails a totally distinct mosaic, so that in general $\tau_e(hk0) \neq \tau_e(\bar{h}\bar{k}0)$.

Constant-path method

The constant-path method leads to a simple physical interpretation of the *e.d.a.* in each case. These physical pictures are given here in detail.

(*a*) *Frontal strip* (F_j) (Fig. 6(*a*))

This lies in an area of type $a_{j,j}$ (*cf.* $a_{3,3}$ in Fig. 5), *i.e.* **i** and **d** enter and leave *via* the same face j. The contours of μl run parallel to the face and rise uniformly as one enters the crystal. If the highest value of μl reached in the block makes exp $(-\mu l)$

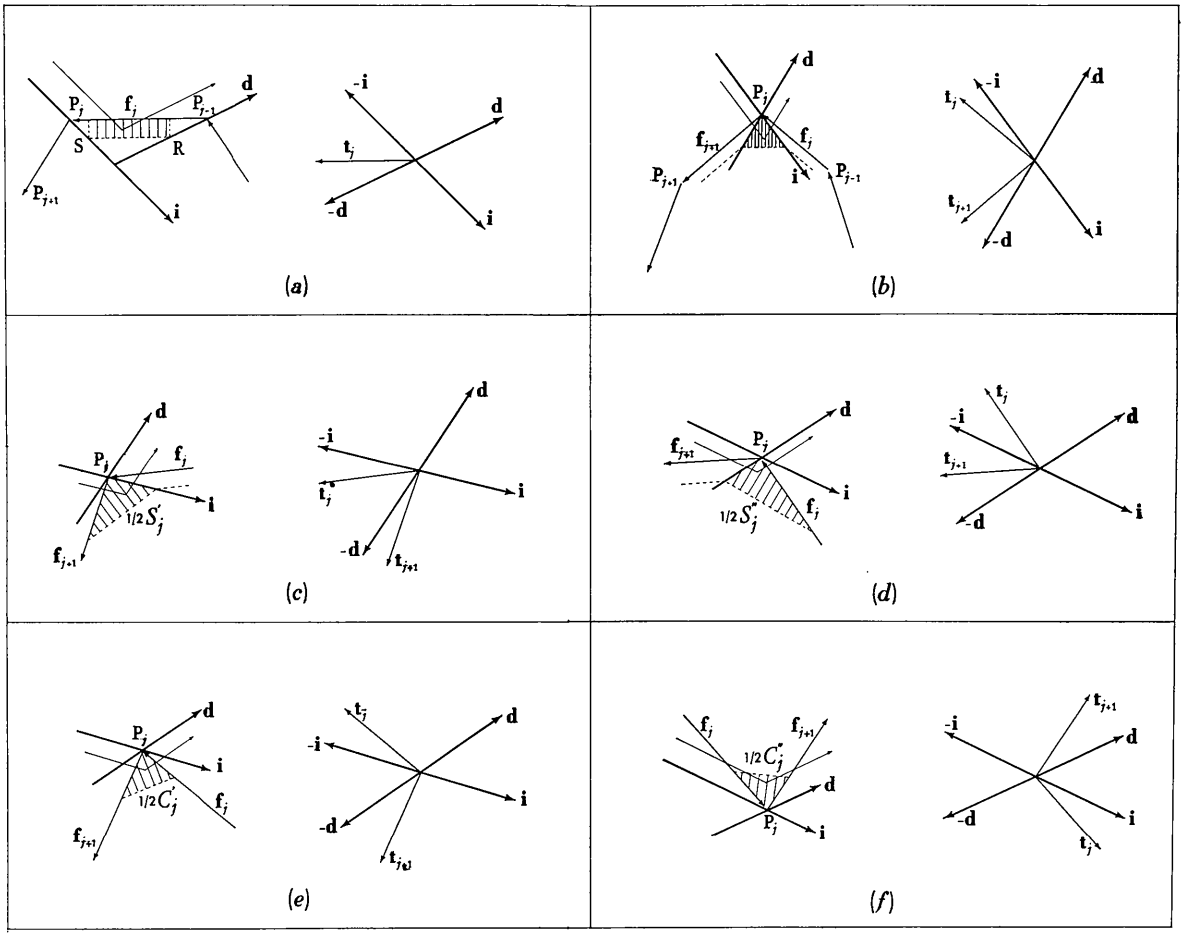

Fig. 6. Physical interpretations of the *e.d.a.* and conditions in the vector fan: (*a*) Frontal strip (F_j). (*b*) Insert (I_j). (*c*) Pre-side face (S_j'). (*d*) Post-side face (S_j''). (*e*) Front corner (C_j'). (*f*) Far corner (C_j'').

negligible, *one can regard the e.d.a. as a strip of completely transparent crystal lying between the exposed face and the contour for which* $\mu l = 1$, *the remainder of the block being regarded as opaque.* It is actually equal to the area of the rectangle based on the $\mu l = 1$ contour, not the trapezium $P_{j-1}P_jSR$, but the difference is usually small. We shall call this a frontal strip (F_j), and the formula for an F-block is the only one to involve a dimension; the formula is expressed in terms of the length of face j ($L_j = \mu f_j$) rather than the length RS of the $\mu l = 1$ contour. The condition in the face vector fan for recognizing an *e.d.a.* of type $a_{j,j}$ is that $\mathbf{t}_j$ falls in the sector $-\mathbf{i}, -\mathbf{d}$.

(*b*) *Insert* (I_j) (Fig. 6(*b*))

This is a region wedged between two F strips which meet at P_j, the $\mu l = 1$ contour bridging the gap, *i.e.* it is of form $a_{j+1,j}$ with both *e.d.a.*$_{j,j}$ and *e.d.a.*$_{j+1,j+1}$ contributing (*cf.* $a_{4,3}$ in Fig. 5). Its *e.d.a.* is twice the area of the triangle so formed. The condition in the face vector fan is that both $\mathbf{t}_j$ and $\mathbf{t}_{j+1}$ fall in the sector $-\mathbf{i}, -\mathbf{d}$.

(*c*) *Pre-side face* (S'_j) (Fig. 6(c))

This is an area abutting on an F_j strip, so that the rays enter S'_j *before* passing out *via* the F strip, *i.e.* it is of the form $a_{j+1,j}$ when *e.d.a.*$_{j,j}$ contributes (*cf.* $a_{5,4}$ in Fig. 5). The $\mu l = 1$ contour reaches the surface in face $j+1$ and joins the contour in the F strip, thus cutting off the corner at P_j. The *e.d.a.* is twice the area of the triangle so formed. The condition in the faces vector fan for the arising of an S'_j contribution is that $\mathbf{t}_j$ falls in sector $-\mathbf{i}, -\mathbf{d}$ and $\mathbf{t}_{j+1}$ falls in sector $-\mathbf{d}, \mathbf{i}$.

(*d*) *Post-side face* (S''_j) (Fig. 6(*d*))

This is an area occurring at the other end of an F strip, so that the rays enter the F_{j+1} strip and exit *via* face j (*i.e.* it is of the form $a_{j+1,j}$ when *e.d.a.*$_{j+1,j+1}$ contributes (*cf.* $a_{3,2}$ in Fig. 5). Again the $\mu l = 1$ contour cuts off corner P_j and the *e.d.a.* is twice the area of the triangle so cut off. The condition in the faces vector fan is that $\mathbf{t}_j$ is in the sector $\mathbf{d}, -\mathbf{i}$ and $\mathbf{t}_{j+1}$ in the sector $-\mathbf{i}, -\mathbf{d}$.

(*e*), (*f*) *Corners* (C'_j *and* C''_j) (Fig. 6(*e*), (*f*))

These are regions occurring alone, *i.e.* the $\mu l = 1$ contour meets adjacent crystal faces, and cuts off the corner at P_j. Again the *e.d.a.*'s are twice the area of the triangles cut off. However, two cases arise:

For a left-hand deflection C'_j is of form $a_{j+1,j}$ when neither *e.d.a.*$_{j,j}$ nor *e.d.a.*$_{j+1,j+1}$ contribute. In this case the optical path must lie wholly inside the *e.d.a.* triangle: it is a corner on the side of the crystal nearest the radiation. We shall call it a *near corner*. The corresponding condition in the face vector fan is that no $\mathbf{t}_j$ fall in the sector $-\mathbf{i}, -\mathbf{d}$.

C''_j occurs at the back of the crystal (*far corner*) and its optical path inside the crystal can lie wholly or partly outside the *e.d.a.* triangle. For a left-hand deflection this is of the form $a_{j,j+1}$ with neither *e.d.a.*$_{j,j}$ nor *e.d.a.*$_{j+1,j+1}$ contributing (*cf.* $a_{6,1}$ in Fig. 5). The face vector fan has no $\mathbf{t}_j$ in the sector $\mathbf{i}, \mathbf{d}$.

The formulae of Table 1 give the *e.d.a.* with an approximation which improves with increase in the absorption of the crystal. In order to assess the accuracy of the given formulae, we have compared the values obtained by the exact formulae and those obtained by the formulae of Table 1.

The accuracy is found to be in agreement with the assertions of Grdenić (1952) and Hendershot (1937). The approximate formulae are applicable when $D = \mu D$, *i.e.* the mean diameter of the crystal multiplied by μ is greater than 4 and the values of ψ_j and φ_j are not small.

Practical procedure

Some examples of section of crystals are drawn in Fig. 7. The very simple rules for recognizing which type of *e.d.a.*$_{p,q}$ contribute to τ_e can easily be for-

Table 2. *Choice of e.d.a.'s contributing to* τ_e *for cross-section of Fig.* 7(*a*)

	Dependent on cross-section				Dependent on cross-section and reflexion ($\Delta_i = 200°$; $\Delta_d = 340°$)								
j	L_j	δ_j	Δ_j	Δ_j'	φ_j	φ_j pos.	ψ_j	ψ_j pos.	R_j	Q_j	R_{j+1}	Q_{j+1}	*e.d.a.*
1	L_1	60	0	90	−250	110	−110	250	−	−	−	−	F_1+I_1
2	L_2	60	60	150	−190	170	−50	310	−	−	+	+	F_2
3	L_3	60	120	210	−130	230	10	10	+	+	+	+	0
4	L_4	60	180	270	−70	290	70	70	+	+	+	+	0
5	L_5	60	240	330	−10	350	130	130	+	+	−	−	0
6	L_6	60	300	390	55	55	190	190	−	−	−	−	F_6+I_6
1	—	—	0	90	−250	110	−110	250	−	−			0

Angles are given in degrees

$L_j = \mu f_j$ (μ in cm^{-1}, f_j in cm)
R_j is the sign of $\varphi_j - \pi$; R_{j+1} is the sign of $\varphi_{j+1} - \pi$
Q_j is the sign of $\pi - \psi_j$; Q_{j+1} is the sign of $\pi - \psi_{j+1}$

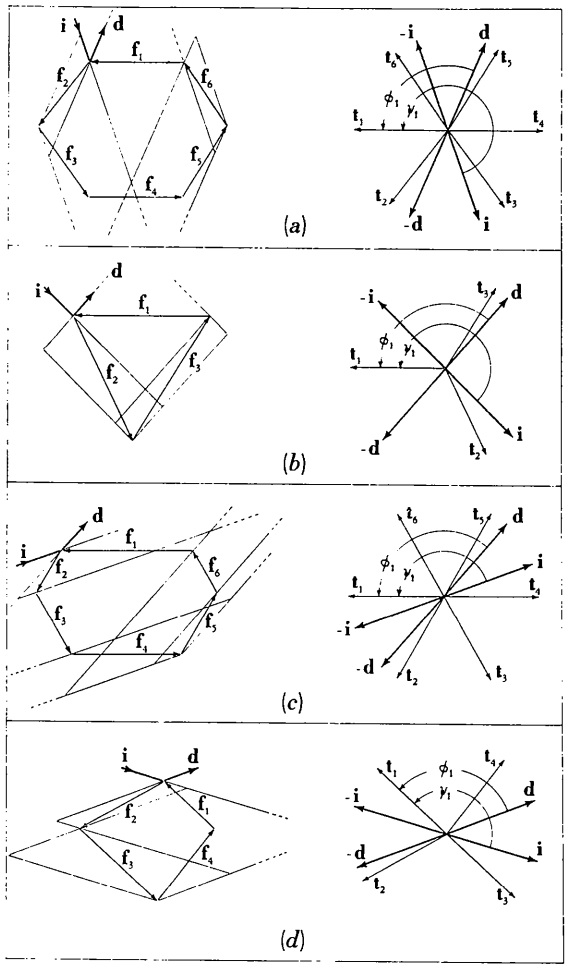

Fig. 7. Some cross-sections and conditions in the vector fan determining the choice of the proper formulae.

Table 3. *Combination of signs of* $\varphi_j-\pi$, $\pi-\psi_j$, $\varphi_{j+1}-\pi$, $\pi-\psi_{j+1}$ *and corresponding e.d.a. (left-handed deflection)*

$\varphi_j-\pi$	$\pi-\psi_j$	$\varphi_{j+1}-\pi$	$\pi-\psi_{j+1}$	
Signs				
R_j	Q_j	R_{j+1}	Q_{j+1}	*e.d.a.*
+	+	−	−	0
+	+	+	−	0
+	+	−	+	0
−	+	−	+	0
−	+	+	+	0
−	+	+	−	C_j'
−	+	−	−	S_j''
+	+	+	+	0
−	−	+	+	F_j
−	−	−	+	0
−	−	+	−	F_j+S_j'
+	−	+	−	0
+	−	−	−	0
+	−	−	+	C_j''
+	−	+	+	0
−	−	−	−	F_j+I_j

mulated. If reference is made to Fig. 7(*a*), the list of angles of Table 2 can be prepared. The choice of the formulae is based only on the combination of signs of $\pi-\psi_j$ and $\varphi_j-\pi$, *i.e.* on the position of $\mathbf{t}_j$ and $\mathbf{t}_{j+1}$ in the vector fan. The combination of signs and corresponding formulae for the cross-sections of Fig. 7 are quoted in the figure itself. A complete list of possible sign combinations and the corresponding formulae is given in Table 3. The procedure of Table 4 can be followed on a computer.

Table 4. *Possible procedure on a computer for calculation of* τ_e

(1) Set list of $L_j(L_1, L_2, \ldots, L_n)$ and $\delta_j(\delta_1, \delta_2, \ldots, \delta_n)$
(2) Set list of $\Delta_j(\Delta_1, \Delta_2, \ldots, \Delta_n, \Delta_1)$
(3) Set list of $\Delta_j'(\Delta_1', \Delta_2', \ldots, \Delta_n', \Delta_1')$
(4) Choose $hk0$ reflexion, *i.e.* calculate ε, $\Delta\mathbf{i}$, $\Delta\mathbf{d}$
(5) Calculate φ_j and transform to φ_j positive; list φ_j
(6) Calculate ψ_j and transform to ψ_j positive; list ψ_j
(7) Calculate signs R_j and Q_j of $\varphi_j-\pi$ and $\pi-\psi_j$; list R_j. Q_j
(8) Combine R_j, Q_j, R_{j+1}, Q_{j+1}
(9) Analyse combination of signs following the scheme:

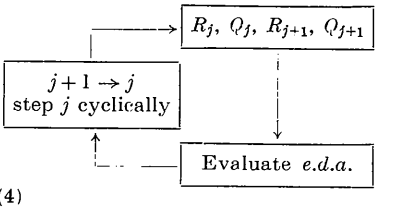

(10) Go to (4)

Extension of the procedure to three-dimensional crystals

The procedure described for a cross-section can be extended to calculate τ_e of the whole crystal. If some approximations are made, the procedure can be applied also to *hkl* reflexions taken with the equi-inclination technique.

The extention to three-dimensional crystals starts from a particular integration procedure of the *e.d.a.*'s. In this integration method it is assumed that the reference system of axes is rotated for each reflexion in such a way as to have the $+x$ axis coincident with $-\mathbf{i}$ and the y axis normal to x and z; z axis is the rotation axis as defined in Fig. 1. Each *e.d.a.* is related to the projection of each side (Fig. 8) on the plane normal to the incident rays. The y axis then represents the line of constant intensity of 'illumination'. Whatever the inclination of the crystal face might be, the energy which reaches the faces must be measured along a line of constant intensity, parallel to the y axis. By analogy the intensity of 'illumination' in three dimensions is proportional to the projection of the crystal face on the plane normal to the incident rays.

Therefore the formulae of Table 1 can be easily extended to three-dimensional crystals. When the crystal has constant cross-section normal to the rotation axis, the transmission factor can be cal-

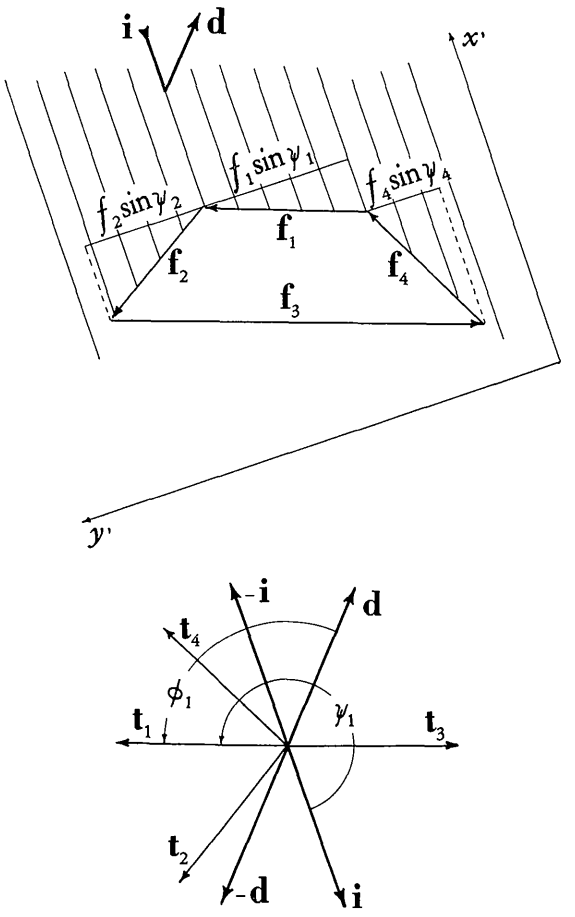

Fig. 8. Intensity of X-rays arriving at each side $\mathbf{f}_n$ referred to lines $-f_n \sin\psi_j$ of constant intensity of 'illumination'.

culated by multiplying the formulae obtained for the cross-section by $\mathscr{H}$, the height of the crystal in cm.

A crystal of varying cross-section is easily dealt with for each of its cross-sectional slices with the same shape. The formulae of Table 1 can then be applied to a slice if one replaces L_j, by

$$\frac{1}{\mu}|\mathbf{P}|\frac{1}{-\sin\psi_j} = \frac{1}{\mu}\frac{H}{2}(L_j+L_j')$$

where $L_j=\mu f_j$ and $L'=\mu f_j'$ (f_j and f_j' are the moduli of two parallel corresponding vectors limiting the slice of height $\mathscr{H}=H/\mu$; for example in Fig. 9 $\mathbf{f}_1$ and $\mathbf{f}_1'$, $\mathbf{f}_2$ and $\mathbf{f}_2'$ and so on). The terms not containing L_j must be multiplied by $\mathscr{H}$. **P** is a vector product, the projection of a crystal face or part of it on the plane normal to the incident rays. The procedure described for a cross-section is followed for each slice with a different outline.

For the equi-inclination technique the diffracting volume can be assumed to be the same as for the corresponding equatorial reflexion with absorption coefficient $\mu \sec\nu$. In order to obtain the projection on the plane normal to the incident rays we form the

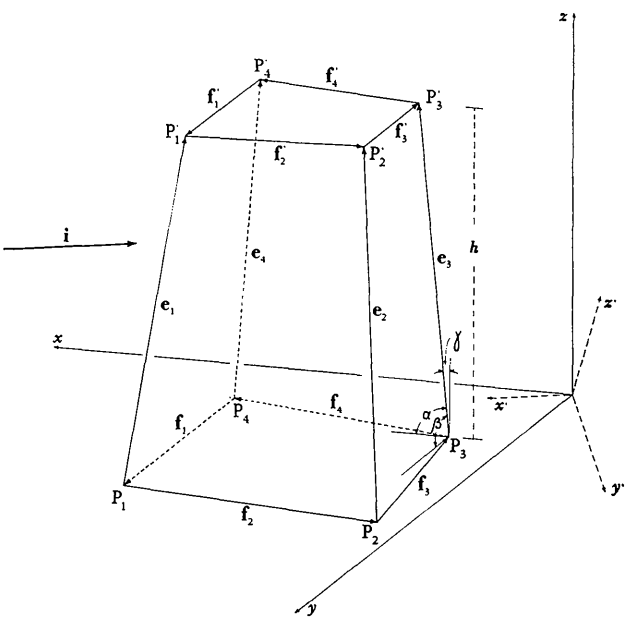

Fig. 9. Slice of a crystal referred to x, y, z, coordinates axes. x', y', z' coordinate axes for equi-inclination setting are also drawn; (y', z') plane is normal to the incident ray **i**.

matrix $[\mathbf{p}]=[\mathbf{0}][\mathbf{N}][\mathbf{e}_j]$ and the matrix $[\mathbf{p}']=[\mathbf{0}][\mathbf{N}][\mathbf{t}_j]$ where

$$[\mathbf{e}_j] = \begin{bmatrix}\cos\alpha\\ \cos\beta\\ \cos\gamma\end{bmatrix},\quad [\mathbf{t}_j] = \begin{bmatrix}1\\0\\0\end{bmatrix},$$

$$[\mathbf{N}] = \begin{bmatrix}-\cos\psi_j & \sin\psi_j & 0\\ \sin\psi_j & \cos\psi_j & 0\\ 0 & 0 & 1\end{bmatrix},$$

$$[\mathbf{0}] = \begin{bmatrix}\cos\nu & 0 & \sin\nu\\ 0 & 1 & 0\\ -\sin\nu & 0 & \cos\nu\end{bmatrix},$$

and $\cos\alpha$, $\cos\beta$, $\cos\gamma$ are direction cosines of the vector $\mathbf{E}_j$ (Fig. 9), *i.e.* the crystal edge joining $\mathbf{f}_j$ to $\mathbf{f}_j'$ at the corner δ_j. The primitive system of axes (right-handed) can be considered as having y parallel to $\mathbf{f}_j$ and $\mathbf{f}_j'$, z parallel to the rotation axis and x normal to both. In the same system $\mathbf{f}_j$ and $\mathbf{f}_j'$ have direction cosines $\cos\beta=1$, $\cos\alpha=\cos\gamma=0$; $\mathbf{E}_j=\mu\mathscr{E}_j$ where $\mathscr{E}_j$ in cm is the length of the crystal edge, ψ_j and φ_j are the same as for the corresponding equatorial reflexion when Υ_2 is substituted for θ, ν is the equi-inclination angle. The projection area becomes

$$|\mathbf{P}| = \frac{L_j+L_j'}{2}\sqrt{(p_2'^2+p_3'^2)}.E_j\sqrt{(p_2^2+p_3^2)}.\sin(\omega'-\omega)\,.$$

p' and p are elements of the one-column matrices $[\mathbf{p}']$ and $[\mathbf{p}]$, $\omega'=\tan^{-1}p_3'/p_2'$ and $\omega=\tan^{-1}p_3/p_2$.

The factor $(1/\mu)(\sec^2\nu/-\sin\psi_j)|\mathbf{P}|$ is substituted for L_j in those terms of Table 1 containing it. The terms of Table 1 not containing L_j are multiplied by

$$(1/\mu)\sec^2\nu E_j\sqrt{(p_2^2+p_3^2)}.\sin(\omega'-\omega)\,.$$

Conclusion

The formulae given are applicable satisfactorily when the values of L_j exceed 4 and when the values of ψ_j and φ_j are not small. The procedure outlined is particularly suitable for application to electronic computers in view of the simple choices and the matrices on which it is based. For crystals having low values of D, the logical foundations of the problem are still valid, but the contributions from the internal areas need to be calculated. The present formulae emphasize the contribution of the surface part of the crystal to the diffracting volume.

APPENDIX

The formulae of Table 1 are derived as follows:

(*a*) *Frontal strip* (F_j) (Fig. 10(*a*))

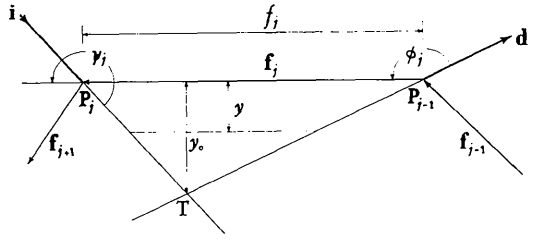

(*a*)

Fig. 10. (*a*) Frontal strip (F_j).

$$e.d.a. = \int_0^{y_0} f_j \left(\frac{y_0 - y}{y_0}\right) \exp\left[-\mu y \left(\frac{1}{\sin\varphi_j} - \frac{1}{\sin\psi_j}\right)\right] dy$$

$$= f_j \int_0^{y_0} \exp(-\mu\alpha y)\, dy - f_j \frac{1}{y_0} \int_0^{y_0} y \exp(-\mu\alpha y)\, dy$$

$$= f_j \frac{1}{\mu\alpha}\left[1 - \frac{1}{\mu\alpha y_0}(1 - \exp(-\mu\alpha y_0))\right].$$

For $\mu\alpha y_0$ large, *i.e.* $\mu(P_jT + TP_{j-1})$ large,

$$e.d.a. = f_j \frac{1}{\mu\alpha}\left(1 - \frac{1}{\mu\alpha y_0}\right)$$

$$= f_j \frac{1}{\mu\alpha} - \frac{\cot(\psi_j - \pi) + \cot(\pi - \varphi_j)}{\mu^2\alpha^2}$$

$$= \frac{1}{\mu^2} \frac{\sin\psi_j \,.\, \sin\varphi_j}{\sin\psi_j - \sin\varphi_j}\left[\mu f_j - \frac{\sin(\varphi_j - \psi_j)}{\sin\psi_j - \sin\varphi_j}\right]$$

$$= \frac{1}{\mu^2} \frac{\sin\psi_j \,.\, \sin\varphi_j}{\sin\psi_j - \sin\varphi_j}\left[L_j + \frac{\sin 2\theta}{\sin\psi_j - \sin\varphi_j}\right].$$

For a contour at a depth t below face j, $l = t\alpha$ and

$$e.d.a. = f_j \frac{t}{\mu l}\left(1 - \frac{t}{\mu l y_0}\right).$$

So if $\mu l = 1$, this becomes

$$= L_j . t(1 - t/y_0)$$
$$= L't$$

where L' is the length of the $\mu l = 1$ contour, *i.e.*

e.d.a. = area of rectangle on L' between the surface and the $\mu l = 1$ contour.

(*b*) *Insert* (I_j) (Fig. 10(*b*))

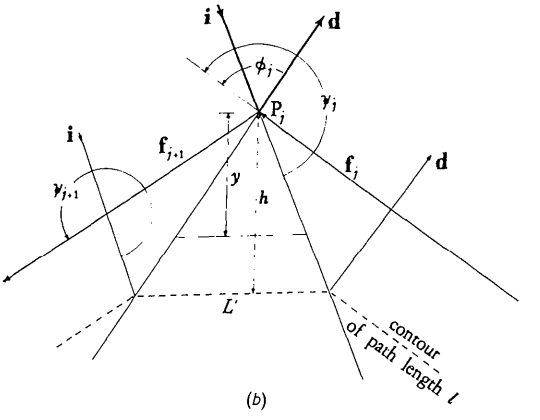

(*b*)

Fig. 10. (*b*) Insert (I_j).

$$e.d.a. = \int_0^Y (y/h) . L' . \exp(-\mu l y/h)\, dy$$

$$= \frac{L'}{h}\left| \exp(-\mu l y/h) \cdot \frac{h^2}{\mu^2 l^2}\left(1 + \frac{\mu l y}{h}\right)\right|_Y^0 .$$

If the triangular region continues interrupted to such a depth Y as to make $\exp(-\mu l Y/h)$ negligible, this becomes:

$$L'h/\mu^2 l^2 ,$$

i.e. twice the area of the triangle cut off by the $\mu l = 1$ contour or, like the frontal strip, is

(length of the $\mu l = 1$ contour) × (maximum depth of this contour below the surface).

$$I_j = \frac{1}{\mu^2}\left(\frac{-\sin\psi_{j+1}}{\sin\varphi_{j+1} - \sin\psi_{j+1}}\right)\left(\frac{\sin\varphi_j}{\sin\varphi_j - \sin\psi_j}\right)\sin 2\theta$$

$$= -\frac{1}{\mu^2} \frac{\sin\varphi_j \,.\, \sin\psi_{j+1} \,.\, \sin 2\theta}{(\sin\psi_j - \sin\varphi_j)(\sin\psi_{j+1} - \sin\varphi_{j+1})} .$$

(*c*) *Pre-side face* (S_j') (Fig. 10(*c*))

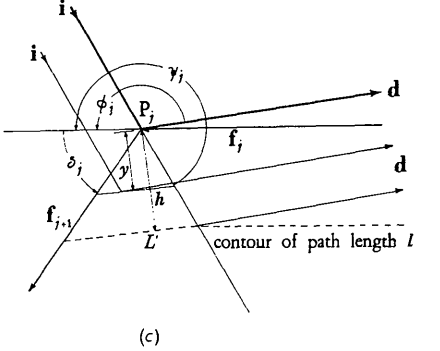

(*c*)

Fig. 10. (*c*) Pre-side face (S_j').

$$e.d.a. = \int_0^Y (y/h).L'.\exp(-\mu l y/h)dy$$
$$= \frac{L'}{h}\left|\exp(-\mu l y/h)\cdot\frac{h^2}{\mu^2 l^2}\left(1+\frac{\mu l y}{h}\right)\right|_Y^0$$
$$= L'h/\mu^2 l^2$$ as for I_j when $\exp(-\mu l Y/h)$ tends to zero at the upper limit of integration; *i.e.*

$e.d.a.$ = twice the area of the triangle cut off by the $\mu l = 1$ contour.

$$S_j' = \frac{1}{\mu^2}\left(\frac{\sin\varphi_j}{\sin\delta_j}\right)\left(\frac{\sin\varphi_j}{\sin\varphi_j - \sin\psi_j}\right)(-\sin\psi_{j+1})$$
$$= \frac{1}{\mu^2}\left(\frac{\sin^2\varphi_j}{\sin\psi_j - \sin\varphi_j}\right)\left(\frac{\sin\psi_{j+1}}{\sin\delta_j}\right).$$

(*d*) *Post-side face* (S_j'') (Fig. 10(*d*))

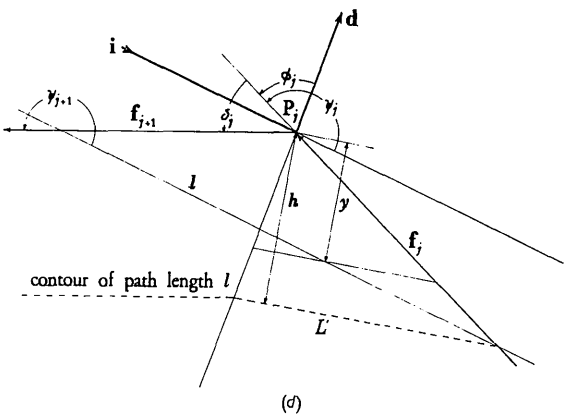

(*d*)

Fig. 10. (*d*) Post-side face (S_j'').

$$e.d.a. = \int_0^Y (yL'/h)\exp(-\mu l y/h)dy$$
$$= L'h/\mu^2 l^2$$ as for S_j' when the upper limit of $\mu l y/h$ is large; *i.e.*

$e.d.a.$ = twice the area of the triangle cut off by the $\mu l = 1$ contour.

$$S_j'' = \frac{1}{\mu^2}\left(\frac{-\sin\psi_{j+1}}{\sin\delta_j}\right)\left(\frac{-\sin\psi_{j+1}}{\sin\varphi_{j+1} - \sin\psi_{j+1}}\right)\sin\varphi_j$$
$$= \frac{1}{\mu^2}\left(\frac{\sin^2\psi_{j+1}}{\sin\varphi_{j+1} - \sin\psi_{j+1}}\right)\left(\frac{\sin\varphi_j}{\sin\delta_j}\right).$$

(*e*) *Front-corner* (C_j') (Fig. 10(*e*))

As before,

$e.d.a. = L'h/\mu^2 l^2$

= twice the area of the triangle cut off by the $\mu l = 1$ contour.

$$C_j' = \frac{1}{\mu^2}\left(\frac{\sin\varphi_j}{\sin\delta_j}\right)\left(\frac{-\sin\psi_{j+1}}{\sin\delta_j}\right)\sin\delta_j$$
$$= -\frac{1}{\mu^2}\frac{\sin\varphi_j.\sin\psi_{j+1}}{\sin\delta_j}.$$

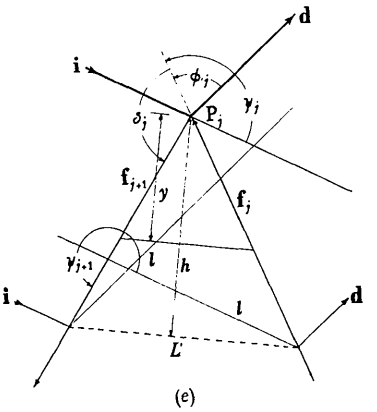

(*e*)

Fig. 10. (*e*) Front-corner (C_j').

(*f*) *Far-corner* (C_j'') (Fig. 10(*f*))

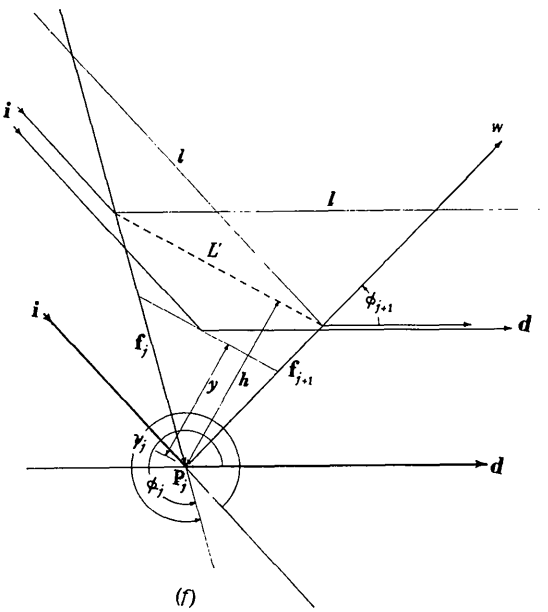

(*f*)

Fig. 10. (*f*) Far-corner (C_j'').

As before,

$e.d.a. = L'h/\mu^2 l^2$

= twice the area cut off by the $\mu l = 1$ contour.

$$C_j'' = \frac{1}{\mu^2}\left(\frac{\sin\varphi_{j+1}}{\sin\delta_j}\right)\left(\frac{-\sin\psi_j}{\sin\delta_j}\right)\sin\delta_j$$
$$= -\frac{1}{\mu^2}\frac{\sin\psi_j.\sin\varphi_{j+1}}{\sin\delta_j}.$$

We are much indebted to Dr D. Rogers, Imperial College, London, for several suggestions regarding the presentation of the paper. We wish to thank also the Consiglio Nazionale delle Ricerche, Rome, for the financial aid given to the present work.

References

ALBRECHT, G. (1939). *Rev. Sci. Instrum.* **10**, 221.
BOND, W. L. (1959). *Acta Cryst.* **12**, 375.
BRADLEY, A. J. (1935). *Proc. Phys. Soc. Lond.* **47**, 879.
BUSING, W. R. & LEVY, H. A. (1957). *Acta Cryst.* **10**, 180.
CARAZZOLO, G. & MAMMI, M. (1956). *Ric. Sci.* **26**, 3342.
EVANS, H. T. (1952). *J. Appl. Phys.* **23**, 663.
EVANS, H. T. & EKSTEIN, M. G. (1952). *Acta Cryst.* **5**, 540.
FERRARI, A., BRAIBANTI, A. & TIRIPICCHIO, A. (1961). *Acta Cryst.* **14**, 1089.
FERRARI, A., BRAIBANTI, A. & TIRIPICCHIO, A. (1963). *Ric. Sci.* **33**, (II–A) 55.
FITZWATER, D. R. (1961). *Acta Cryst.* **14**, 521.
FRASSON, E. (1958). *Gazz. chim. ital.* **88**, 779.
FRASSON, E. & BEZZI, S. (1958). *Gazz. chim. ital.* **88**, 627.
FRASSON, E. & BEZZI, S. (1959). *Acta Cryst.* **12**, 536.
GRDENIĆ, D. (1949). *Glasn. mat. fiz. astr.* (II) **4**, 149.
GRDENIĆ, D. (1952). *Acta Cryst.* **5**, 283.
GRDENIĆ, D. (1956). *Acta Cryst.* **9**, 540.
HENDERSHOT, O. P. (1937). *Rev. Sci. Instrum.* **8**, 324.
HENSHAW, D. (1958). *Acta Cryst.* **11**, 302.
HOWELLS, R. G. (1950). *Acta Cryst.* **3**, 366.
JOEL, N., VERA, R. & GARAYCOCHEA, I. (1953). *Acta Cryst.* **6**, 465.
ROGERS, D. & MOFFETT, R. H. (1956). *Acta Cryst.* **9**, 1037.
WELLS, M. (1960). *Acta Cryst.* **13**, 722.

Acta Cryst. (1965). **18**, 55

The Crystal Structure of Longifolene Hydrochloride

BY A. F. CESUR* AND D. F. GRANT

Viriamu Jones Laboratory, University College, Cardiff, Wales

(*Received* 16 *January* 1964)

Longifolene hydrochloride crystallizes in the space group $P2_12_12_1$ with $a=8{\cdot}505$, $b=9{\cdot}760$ and $c=16{\cdot}674$ Å. The structure, originally solved in projection by the isomorphous replacement method, has been confirmed by three-dimensional methods. Coordinates have been given to the 25 hydrogen atoms in the molecule, and the structure has been refined by least-squares methods. New values for the bond lengths and bond angles are given and the strain in the molecule is discussed.

1. Introduction

Longifolene, $C_{15}H_{24}$ (Fig. 1(*b*)), is a sesquiterpene whose molecular constitution was virtually unknown (Simonsen & Barton, 1952) until it was determined by Moffett & Rogers (1953) (Moffett, 1954) from the X-ray study in projection of the crystal structure of longifolene hydrochloride (Fig. 1(*a*)) and confirmed by the chemical evidence of Naffa & Ourisson (1953) (Simonsen & Ross, 1957). As a result of considerable overlap in the projections of the structure, some aspects of this X-ray work were not satisfactory (see below), and Barton & Mayo (1957) suggested that further chemical evidence was needed to confirm the proposed structure. More recently, longifolene has been synthesized by Corey, Ohno, Vatakechery & Mitra (1961), who state that the chemical facts alone did not constitute a proof of the molecular structure.

In this paper, a complete three-dimensional analysis of the crystal structure of longifolene hydrochloride is described, removing the possible doubts about the previous X-ray work and confirming in detail the structure previously found. As only a brief account of the two-dimensional work has been given, it is reviewed in the next paragraph.

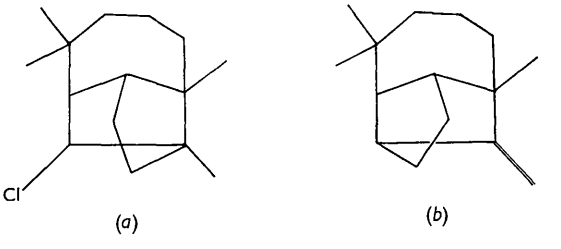

Fig. 1. (*a*) Longifolene hydrochloride. (*b*) Longifolene.

2. The previous work by Moffett & Rogers

The crystals of longifolene hydrochloride and hydrobromide were found to be isomorphous in the space group $P2_12_12_1$. The coordinates of the chlorine and bromine atoms were found from the (100) and (010) Patterson projections and the method of isomorphous replacement was used to determine the signs of 130 out of the 154 observed $0kl$ reflexions and the signs of 104 out of 126 observed $h0l$ reflexions. The electron density maps for these two projections were calculated for the hydrochloride. It was not possible to fit any of the then proposed chemical models to these maps.

Moffett & Rogers proceeded without making any assumptions about the chemical structure and,

* Present address: Fen Fakültesi, Ankara, Turkey.